

DEEP 1.4 GHZ VLA OBSERVATIONS OF THE RADIO HALO AND RELIC IN ABELL 2256

T. E. CLARKE

Naval Research Laboratory, Code 7213, 4555 Overlook Ave SW, Washington, DC, 20375 and
Interferometrics Inc., 13454 Sunrise Valley Dr., Suite 240, Herndon, VA, 20171

AND

T. A. ENSSLIN

Max-Planck-Institut für Astrophysik, Karl-Schwarzschild-Str.1, Postfach 1317, 85741 Garching, Germany
Draft version May 17, 2018

ABSTRACT

We present deep VLA observations of the merging galaxy cluster Abell 2256. This cluster is known to possess diffuse steep spectrum radio relic emission in the peripheral regions. Our new observations provide the first detailed image of the central diffuse radio halo emission in this cluster. The radio halo extends over more than 800 kpc in the cluster core, while the relic emission covers a region of $\sim 1125 \times 520$ kpc. A spectral index map of the radio relic shows a spectral steepening from the northwest toward the southeast edge of the emission, with an average spectral index between 1369 MHz and 1703 MHz of $\alpha = -1.2$ across the relic. Polarization maps reveal high fractional polarization of up to 45% in the relic region with an average polarization of 20% across the relic region. The observed Faraday rotation measure is consistent with the Galactic estimate and the dispersion in the rotation measure is small, suggesting that there is very little contribution to the rotation measure of the relic from the intracluster medium. We use these Faraday properties of the relic to argue that it is located on the front side of the cluster.

Subject headings: galaxies:clusters:individual(A2256)— radiation mechanisms: non-thermal— shock waves— magnetic fields

1. INTRODUCTION

In the hierarchical model of structure formation, objects form from the gravitational collapse of initial density enhancements and subsequently grow through accretion and mergers. Numerical simulations of structure formation show that clusters of galaxies are found to preferentially form at the intersections of large filamentary structures (West et al. 1991; Katz & White 1993). Due to the high-density environment in which they reside, clusters of galaxies are expected to undergo several merger events during their lifetime. These merger events are highly energetic ($10^{63} - 10^{64}$ ergs) and thus provide a significant energy input into the intracluster medium (ICM). Large scale structure simulations (Miniati et al. 2000) as well as 3D MHD/N-body simulations (Roettiger et al. 1999a,b; Dolag et al. 1999) find that the shocks and turbulence associated with a major cluster merger event can significantly amplify the intracluster magnetic field strength and accelerate relativistic particles which, in the presence of a magnetic field, emit synchrotron emission.

Radio observations toward a number of galaxy clusters reveal the presence of large regions of diffuse radio emission which extend over scales of > 600 kpc in the ICM and have no obvious optical counterpart (see review by Giovannini & Feretti 2002). This emission appears to fall in two categories: *halos* which are centrally located in the cluster, relatively regular in shape, and unpolarized, and *relics* which are peripherally located, fairly elongated and irregular, and often highly polarized (Feretti & Giovannini 1996). In an X-ray flux limited cluster sample, Giovannini et al. (1999) find that 5% of clusters contain a known radio halo and 6% contain a detected radio relic.

The presence of these large regions of diffuse synchrotron emission reveals the large scale distribution of relativistic particles and magnetic fields in the intracluster medium. Despite extensive searches through the 1.4 GHz NRAO VLA Sky Survey (Giovannini et al. 1999) and the 330 MHz Westerbork Northern Sky Survey (Kempner & Sarazin 2001) as well as a number of targeted searches for radio halos and relics (Kassim et al. 2001; Giovannini & Feretti 2000; Liang et al. 2000; Venturi et al. 2000; Reid et al. 1999; Slee & Roy 1998; Feretti et al. 1997; Harris et al. 1993; Andernach et al. 1988; Cordey 1985; Hanisch et al. 1985) there are still a relatively small number of clusters known which host this diffuse emission.

Galaxy clusters which are confirmed to contain diffuse radio emission also show significant evidence of merger activity. The clusters which contain radio halos tend to be very X-ray luminous, massive clusters (Colafrancesco 1999; Liang et al. 2000; Buote 2001) which display a significant amount of X-ray substructure. Although this suggests that the merger event is the trigger for the diffuse emission, it should be noted that while only $\sim 5\%$ of all galaxy clusters in a complete X-ray flux limited sample appear to contain diffuse emission, more than 40% of clusters show evidence of merger activity (Jones & Forman 1999). On the other hand, Giovannini & Feretti noted that the detection rate of diffuse emission is significantly enhanced for high X-ray luminosity clusters where it reaches $\sim 33\%$ for a sample with X-ray luminosity larger than 10^{45} ergs s^{-1} . Buote (2001) suggests that this is due to the preferential formation of diffuse radio emission in massive clusters which are currently experiencing violent mergers.

In this paper we present new radio maps of the diffuse

emission in Abell 2256. The aim of our investigation is to use this cosmic laboratory to study details of plasma physics, magneto-hydrodynamics, and eventually particle physics. In particular, the goal of the polarimetry observations is to use the Mpc scale radio relic emission to investigate statistical properties of the ICM magnetic field. This first paper presents the data and a discussion of the geometry of the system. The application of statistical tools to the data to extract information on magneto-hydrodynamical turbulence, particle acceleration, etc. is left to follow-up publications. Unless otherwise noted, we adopt WMAP cosmological parameters Bennett et al. (2003) $H_0=71 \text{ km s}^{-1} \text{ Mpc}^{-1}$, $\Omega_\Lambda=0.73$, and $\Omega_m=0.27$. At the redshift of Abell 2256 ($z=0.0594$), this corresponds to a linear scale of 1.13 kpc/arcsec.

2. TARGET CLUSTER: ABELL 2256

Abell 2256 is a rich, nearby ($z = 0.0594$) galaxy cluster which was one of the first targets observed by ROSAT. Analysis of these observations (Briel et al. 1991) revealed significant X-ray substructure in the cluster. The X-ray surface brightness distribution shows two separate X-ray peaks that suggest it is undergoing a merger event. The X-ray temperature map of the cluster (Briel & Henry 1994) indicated that the infalling component is cooler than the main cluster body and that there are two hot regions roughly perpendicular to the merger axis. These hot regions appear similar to those seen in simulations of merger events where the merger has not yet proceeded past core passage (Schindler & Müller 1993; Roettiger et al. 1997). More recent *Chandra* observations of the cluster by Sun et al. (2002) provide much more detail on the cluster merger state. They find a sharp surface brightness feature south of the merging subcluster. The temperature map of the region shows a temperature jump across the edge with the cooler gas associated with the subcluster. Sun et al. suggest that the structure south of the subcluster core is similar to the “cold fronts” seen in merging clusters such as Abell 2142 (Markevitch et al. 2000) and Abell 3667 (Vikhlinin et al. 2001). These features are thought to delineate the contact surface between the undisturbed cool core of a merging system and the hot thermal gas through which they are moving. The *Chandra* data also reveal a third component to the X-ray structure in the system. Sun et al. (2002) find an X-ray “shoulder” located $2'$ east of the main X-ray peak in the core of the cluster. This structure may be the remnant of an old merging component in the cluster, or may represent substructure in the core of the primary.

Radial velocity studies of 277 cluster member galaxies by Berrington et al. (2002) find that the cluster is composed of three substructures. The two main galaxy groups correspond spatially to the primary cluster and the infalling subcluster. The third group is located to the north of the cluster core and apparently represents a previously unknown merging system. Berrington et al. suggest that the subcluster is infalling onto the primary cluster from the northwest, while the newly identified group is located on the near side of the system and is merging from the north. They interpret the radio relic emission as the result of the merger of the group with the other systems. A similar distribution of three merging components was also identified by Miller et al. (2003).

They suggest a slightly different scenario where the merging group has already passed through the system from the south close to the line of sight and is currently located on the far side of the system. On the other hand, Miller et al. point out that the low velocity dispersion of the group does not appear to be consistent with a post-merger scenario, although they suggest that the low velocity dispersion may be an artifact of the galaxy assignment algorithm.

Radio observations of Abell 2256 (Bridle & Fomalont 1976; Masson & Mayer 1978; Bridle et al. 1979; Röttgering et al. 1994) show that the cluster is host to a remarkable assortment of sources. There are at least four head-tail galaxies in the cluster, one of which has a narrow straight tail that extends for at least 480 kpc (Röttgering et al. 1994, hereafter R94). The northwest region of the cluster contains two large, sharp-edged radio relics which appear to be roughly at the location of the infalling cooler subcluster. Bridle & Fomalont (1976, hereafter BF76) also suggest the possibility of a cluster-center radio halo based on Westerbork 610 MHz observations. These observations are discussed in more detail in § 4.

3. RADIO OBSERVATIONS AND DATA REDUCTIONS

Abell 2256 was observed at four frequencies across the 1.4 GHz band using the National Radio Astronomy Observatory’s VLA¹ in the C and D configurations. The observational parameters are summarized in Table 1. All observations include full polarization information and used 3C286 as the primary flux density calibrator and absolute electric vector position angle calibrator. Phase calibration was obtained from the nearby calibrator 1803+784, and multiple observations of 1458+718 over a large range of parallactic angles were used to calibrate the polarization leakage for each antenna. Observations at 1703 MHz on 1999 April 29 were severely impacted by radio frequency interference during the first 1.5 hours of observation and this data has been removed from the analysis.

Data were calibrated and reduced using NRAO’s Astronomical Image Processing System (AIPS). The data were calibrated following standard procedures. Wide-field, 3-D imaging techniques were implemented within the AIPS task IMAGR to allow us to compensate for the non-coplanar geometry of the VLA (Cornwell & Perley 1992). Imaging used a total 22 facets to cover the primary beam and bright outlying sources. We also included the multiresolution clean option within the AIPS IMAGR task to allow us to better image the complex diffuse structure in this system. Each data set was self-calibrated using phase-only followed by amplitude and phase solutions. The final images used for spectral index and Faraday rotation measures were created using a suitable taper within the AIPS task IMAGR followed by a convolution with a Gaussian to exactly match each beam. The polarized intensity, fractional polarization, and polarization position angle images were created from the Stokes Q and U images at a given frequency. The Faraday rotation measure (RM) image was determined from the four frequencies around 1.4 GHz and provides an un-

¹ NRAO is operated by Associated Universities Inc., under a cooperative agreement with the National Science Foundation.

ambiguous measurement for $|\text{RM}| < 300 \text{ rad m}^{-2}$

4. TOTAL INTENSITY PROPERTIES

Previous radio observations of Abell 2256 (Bridle & Fomalont 1976; Röttgering et al. 1994; Miller et al. 2003) have revealed that it contains very complex radio emission. BF76 attached alphabetic designations to numerous radio sources in the cluster. These designations were expanded in subsequent papers by Bridle et al. (1979), and R94 as more sensitive and higher resolution data became available. R94 designate 34 individual sources in the direction of the cluster. We will not discuss the majority of the sources in this paper as we concentrate on lower resolution, high surface brightness sensitivity images of the extended diffuse emission. A detailed discussion, including high resolution radio overlays on optical images of the sources is given in Miller et al. (2003). Combining their optical data with that of Berrington et al. (2002), Miller et al. have velocity measurements for 49 of the 54 candidate cluster radio galaxies and find that 40 of these are confirmed cluster members.

In the top left panel of Figure 1 we show the 1369 MHz D configuration image of Abell 2256 covering a region of $2.6 \times 2.5 \text{ Mpc}$. The well-known radio relic region (G and H in BF76) is visible as the bright elongated region to the north-west. Our observations show the first clear detection of additional diffuse emission (at a much lower surface brightness) centered to the south-east of the relics. This emission is co-incident with the diffuse emission seen around source D by BF76 and is referred to as the halo below. A third region of interest in Abell 2256 is associated with the Z-shaped source F in the BF76 notation. This source is visible on the north-eastern edge of the radio halo and has been noted for its unusual shape and spectral properties in several papers (Masson & Mayer 1978; Bridle et al. 1979; Röttgering et al. 1994; Miller et al. 2003).

4.1. Relic Emission

The radio relic emission is seen to concentrate into two bright regions (G and H) which are surrounded by an extended region of diffuse emission. Our new observations are sensitive to much lower surface brightness emission than those of R94 and show that the relics are even more extensive than previously known. The entire relic region covers an area of roughly 16.9×7.8 ($\sim 1125 \times 520 \text{ kpc}$) and is bounded by a relatively steep surface brightness drop on all sides, although the southeast edge appears particularly sharp as pointed out by R94. In the analysis that follows we will discuss a single relic region which covers sources G and H as well as the extended diffuse emission which surrounds them. Higher resolution observations of the relic region by R94 and Miller et al. (2003) show that there are a number of compact radio sources and two head-tail galaxies in the area covered by the relic emission. In Figure 2 we show the VLA C configuration 1369 MHz image of the cluster. The diffuse emission is not visible due to the lack of short baselines, but the relic can be seen to contain a number of bright synchrotron filaments of width $\sim 30 \text{ kpc}$. We also provide source labels in Figure 2 for all sources discussed in the text.

We have estimated the total flux in the radio relic region using several different methods in order to account

for the influence of the additional source flux from the discrete sources. Our first method involved subtracting the total flux of the compact and head-tail galaxies in the region (using the data from Table 2 of Miller et al. 2003 or Table 3 of R94) from the flux of the region in our D configuration observations. This method may produce an overestimate of the relic flux as there are several compact sources in the relic region which do not have flux measurements in Miller et al. (2003). Additionally, the high-resolution data of Miller et al. (2003) may resolve out some of the tail of the extended head-tail source C. This is seen both in a visual comparison of their Figure 1 with Figure 10 of R94 as well as by the flux comparison between the two papers which shows $\sim 13\%$ more flux in R94. A second estimate of the relic flux was obtained by adding up the flux of the compact sources seen in the region of the relic in our C-configuration observations and removing that from the total flux in the D-configuration observations. A third estimate was obtained from the multiresolution clean image where we identified the delta-function clean components associated with the compact and head-tail sources in the central regions of the cluster and subtracted those from the final maps in order to produce a radio map containing mainly the diffuse radio emission. We note that there is significant filamentary structure within the relics as well as extended structure around several of the radio galaxies so a straight filtering of data at short baselines will not properly meet our goal of removing just the discrete source components. We show this map in Figure 3. Although this method does a good job of removing all the compact sources and the majority of the more extended discrete sources, there are still a few regions of extended emission associated with sources A, B, and F (in the notation of BF76). This excess residual emission is not important for determining the relic flux but is discussed below for the determination of the halo flux.

All three methods produce remarkably similar flux estimates. Including only the standard noise error estimate we find a total 1369 MHz flux of $462 \pm 0.8 \text{ mJy}$ for the entire relic region using the average of the three measurements. Due to measurement uncertainties in removing the discrete sources we estimate the error in the total flux to be roughly $2\%^2$.

4.2. Halo Emission

In addition to the large region of radio relic emission, our new observations provide the first detailed image of the diffuse central halo emission in Abell 2256. This emission is roughly centered on source D as originally pointed out by BF76. The size and morphology of the halo emission is difficult to determine due to the presence of the discrete sources and apparent overlap of the halo and relic emission regions. Nevertheless, the improved sensitivity of our observations shows that the halo is significantly larger than seen by Bridle & Fomalont. We use the roughly circular region of the halo in Figure 1 that runs counter-clockwise from the north-east to south-west and estimate the radius of the halo emission to be 6.1 , or 406 kpc . The edges of the halo are much more diffuse

² Note that the flux errors presented here and for the halo emission only refer to measurement errors from the given maps and do not include an assessment of errors from the map-making process.

than those of the relic and it is possible that deeper observations will reveal that the halo emission is even more extended.

We used similar methods to those described above to estimate the total flux of the halo and the systematic error due to the removal of contaminating sources. One difference in the multiresolution clean estimate of the halo flux was that we corrected for the large residual flux left in Figure 3 from sources A, B, and F. This was done by subtracting the total flux in the areas of excess around each source and then adding back in a flux estimate for the region excised based on the average halo flux in the region of each source.

Due to the large flux contributions and extended sizes of the sources embedded in the halo, the three methods of estimating the halo flux show larger scatter. Including the standard noise estimate we find a total 1369 MHz flux of 103.4 ± 1.1 mJy for the halo. The uncertainties in this measurement are on the order of 20%.

5. SPECTRAL INDEX

We have undertaken wide-field multiresolution clean imaging of an additional three frequencies from our D-configuration observations. These images are shown in panels b (1417 MHz), c (1512.5 MHz), and d (1703 MHz) of Figure 1. The radio relic emission shows very little change across the four frequencies with the only visible difference being the loss of the small low surface brightness extension to the north-east of the eastern relic edge in the higher frequency maps. The halo shows significant change across the frequencies with the majority of the southern portion of the halo missing in the 1703 MHz observations. Unfortunately, due to radio frequency interference at 1703 MHz the noise level in our highest frequency map is roughly 13% higher than that of the other 3 frequencies. We note also that the uv coverage across the four frequencies changes resulting in a loss of sensitivity to the largest scale emission in the 1703 MHz data. It is quite possible that the missing southern portion of the halo emission at 1703 MHz is the result of these instrumental limitations.

To make the spectral index map we smoothed the individual total intensity maps with a circular $53''$ Gaussian beam. Due to the large size of Abell 2256, each map was corrected for the attenuation of the primary beam of the VLA antennas. After computing the spectral index map, it was blanked anywhere that the noise on either of the two input maps fell below the 3σ level ($\sigma_{1369} = 1.0 \times 10^{-4}$ Jy, $\sigma_{1703} = 1.1 \times 10^{-4}$ Jy). We show the spectral index map between 1369 MHz and 1703 MHz in Figure 4. Overall the spectral index of the relic region is fairly uniform with an average spectral index ($S_\nu \propto \nu^\alpha$) of $\alpha = -1.2$. The extended tail of source C appears as a steeper spectrum region in the figure. The spectral steepening along the tail of this source is consistent with the measurements of R94. Assuming a uniform spectral index of $\alpha = -1.2$ for the relic, we estimate the total 1.4 GHz rest-frame power of the relic region is $P_{1.4} = 3.6 \times 10^{24}$ W Hz $^{-1}$.

There is some evidence for a spectral steepening from the NW edge of the relic toward the SE edge. To look at the trend of spectral index with location across the relic we have set up 18 strips of width $6'.5$ parallel to the long edge of the relic (i.e. at a position angle of 53°).

We have determined the average spectral index in each of the strips and plot these in Figure 5 where strip 1 is located toward the SE edge of the relic and strip 18 is near the NW edge. The first eight strips (covering roughly $2'.5$) show a roughly linear increase in spectral index from $\alpha = -1.5$ to $\alpha = -1.0$. The remainder of the strips (covering $\sim 3'$) show relatively constant spectral index of $\alpha \sim -0.98$. A careful examination of Figure 4 of Bridle et al. (1979) shows a similar spectral trend along the relics between frequencies of 1415 MHz and 610 MHz. We note that the spectral index we measure for the relics between 1369 MHz and 1703 MHz is significantly steeper than that reported by R94 between 1446 MHz and 327 MHz and suggests a spectral flattening of the relics to lower frequencies. We will undertake a more detailed spectral analysis of the diffuse emission in a subsequent paper where we present data over a much larger range of wavelengths. We defer a detailed discussion of the spectral index implications to that paper.

The diffuse radio halo is a low surface brightness source with several large bright sources superimposed. Across the short frequency baseline presented in this paper it is very difficult to measure the halo flux with sufficient accuracy to estimate the spectral index. We discuss above the effects of uv coverage on the diffuse emission, and in § 4.2 we estimate the uncertainty in the 1369 MHz halo flux is on the order of 20%, thus we defer a new measurement of the halo spectral index to a later paper. Using a longer frequency baseline between 151 MHz and 610 MHz, Bridle et al. (1979) estimate the halo spectral index is $\alpha = -1.8$. Using this spectral index together with our measured 1369 MHz flux, we estimate the total 1.4 GHz rest-frame power of the halo region is $P_{1.4} = 8.2 \times 10^{23}$ W Hz $^{-1}$.

Liang et al. (2000) showed that the 1.4 GHz rest-frame radio power of well-confirmed radio halos is correlated with the X-ray luminosity (L_X) of the host cluster. We show in Figure 6 the plot of the bolometric X-ray luminosity versus 1.4 GHz rest-frame halo power for known radio halos. Our new measurement of the halo power for A2256 (star) yields a halo power roughly 4 times higher than the previous published halo power from Feretti (2002) (open triangle) and move A2256 from an outlier position onto the correlation found by Bacchi et al. (2003).

The third steep-spectrum radio source in Abell 2256 is the Z-shaped source located on the eastern side of the halo (source F in the notation of BF76). Miller et al. (2003) find that the eastern component (F3) is associated with a cluster member galaxy and is probably not related to the remainder of the source. The central portion of the source (F2) appears to have a shell-like morphology (Röttgering et al. 1994; Miller et al. 2003) and may be a member of the phoenix radio relic class (Kempner et al. 2004) which are shock compressed old radio lobes (so called radio ghosts) of former radio galaxies. We find a steep spectral index of $\alpha = -2.5 \pm 0.2$ for the F2 portion of the source between 1369 MHz and 1703 MHz.

6. POLARIZATION PROPERTIES

The radio observations of Abell 2256 presented in this paper were taken in full polarization mode to allow us to investigate the polarization properties of the cluster. For each of the four frequencies, we have obtained im-

ages in all four Stokes parameters. We have used the Stokes Q and U images to make maps of the total linear polarization in this system. The polarization percentage map was made by taking the ratio of the linear polarization map and the total intensity map and blanking the output map anywhere that either the total intensity or linear polarization fell below 3σ .

In Figure 7 we display the fractional polarization of the radio emission at 1369 MHz. We have included the outer contours of the 1369 MHz total intensity emission in the plot for comparison with Figure 1. We see that the discrete sources A, B, and P (in the R94, notation) are polarized at the level of 1–5%. This polarization fraction is typical for extragalactic radio sources observed at this frequency (Slee et al. 1994; Mesa et al. 2002). The polarization map also reveals that the entire radio relic shows high levels of polarization while there is no detectable polarization associated with the radio halo emission or the Z-shaped source.

The linear polarization of the radio relic emission reaches a fractional polarization of up to 45% in the interior region with an average polarization over the entire relic of 20%. This average polarization fraction is consistent with the value reported by Bridle et al. (1979). There are two extended regions in the relic where the polarization drops to the 3–5% level (blue regions in Figure 7). In Figure 8 we show the region of the relic emission with the Faraday-corrected magnetic field vectors plotted on the total intensity greyscale and contour image at 1369 MHz. At the resolution of these images, the magnetic fields show large scale order over distances of up to $7'$ (475 kpc). The magnetic field over a large region in the central part of the relic is oriented roughly parallel to the long axis of the emission. The polarization vectors show a change in the field orientation in the brightest region of the western portion of the relic near the head-tail galaxy C. This region coincides with the location of the bright X-ray feature seen around the region P₂ in the notation of Sun et al. (2002). We show an overlay of the diffuse radio emission (after subtraction of discrete sources) and the smoothed X-ray emission in Figure 9.

In any relic formation scenario the magnetic fields become aligned with the shock plane. That means that seen with some inclination, even an originally isotropic distribution of fields would exhibit a preferred direction, observable by a global polarization signature. We find that the averaged polarized emission is still at the 20% level over a larger region of the relic. The averaged polarization B-vector over the sub-region of the relic used to measure the polarization fraction is aligned on a position angle of 10° (measured east of north). The polarization fraction indicates an inclination between the shock plane and plane of sky of $\sim 45^\circ$ (Enßlin et al. 1998) with the average B-vector lying in both planes. Note however, that since the relic shows large scale magnetic structures with sizes comparable to the relic, the assumption of an initially isotropic field distribution within the relic volume needs not be completely fulfilled.

Our observations do not show any significant polarization for the diffuse halo emission. Using the 3σ noise level in our polarization images we place a conservative upper limit of 16% on the polarization of the halo. Due to the low surface brightness of the halo,

this upper limit is higher than that for the Coma halo ($< 10\%$, Feretti & Giovannini 1998). More strict upper limits on halo polarization have been obtained for Abell 2219 ($< 6.5\%$, Bacchi et al. 2003), Abell 2163 ($< 4\%$, Feretti et al. 2001), and 1E0657–57 ($< 6.5\%$, Liang et al. 2000). The first clear detection of polarization in a halo area has recently been presented by Govoni et al. (2005) where a number of filaments polarized at levels of 20%–40% were detected. Similarly, the lack of polarized emission in the region of the Z-shaped source places an upper limit of 2% on its linear polarization.

We have combined the polarization data of all four frequencies to produce a Faraday rotation measure (RM) map which we show in Figure 10. The map was created by tapering the Stokes Q and U images at all four frequencies to similar beams then convolving each image to a $53'' \times 45''$ beam at a position angle of 45° . The rotation measure was calculated using a weighted fit of the position angle to the wavelength squared. The output map was blanked anywhere that the position angle errors at any input frequency were greater than 15° .

The RM map shows a remarkably uniform distribution across the relics with a mean rotation measure of -44 rad m^{-2} and a dispersion of 7 rad m^{-2} . At the position of Abell 2256 ($\ell_{II} = 111^\circ 09'$, $b_{II} = 31^\circ 7'$) the Galactic RM is expected to be about $-4 \pm 37 \text{ rad m}^{-2}$ based on an average of the 7 sources within 15° in the RM catalog of Simard-Normandin et al. (1981). The Faraday rotation measure across the relic is consistent with being Galactic in origin and thus any cluster component is likely to be very small. This suggests that the relic is on the near side of the cluster and is not experiencing significant Faraday rotation from the intracluster medium.

7. DIFFUSE RADIO EMISSION AND THE GEOMETRY OF THE MERGER

In the following we try to understand the three dimensional geometry of the merger by comparing the observed properties of the radio halo and relic to current theoretical concepts of their nature.

Our spectral index measurements of the radio relic reveal that the spectrum across the 20 cm band seems to steepen from $\alpha = -0.98$ near the NW edge to $\alpha = -1.5$ near the SE edge. Radio relics in clusters are believed to be a direct tracer of merger shock waves. They could be due to Fermi acceleration of relativistic electrons at a merger shock wave (Enßlin et al. 1998; Roettiger et al. 1999a; Miniati et al. 2001) or due to compression and re-ignition of fossil radio plasma (so called *radio ghosts* or *ghost cavities*, Enßlin 1999; Enßlin & Gopal-Krishna 2001; Enßlin & Brüggen 2002; Hoeft et al. 2004). In the notation of Kempner et al. (2004) the former are the “radio gischt” or “radio tsunami”, while the latter are the “radio phoenix”. Given the Mpc size of the relic structure in A2256, the second explanation is unlikely since the radiative energy losses during the time it takes to compress a several hundred kpc sized radio ghost would remove most of electrons responsible for the observable radio emission. Therefore, it is more likely that we are witnessing direct shock acceleration in the relic region. In this case, one expects a trend in the spectral index of the radio emission from flatter to steeper as one moves from the current shock location to the trailing edge (in

the observers projection) (Enßlin et al. 1998). The spectral index profile in Figure 5 therefore suggests that the part of the merger shock wave associated with the relic probably travels from the SE toward the NW.

Cluster radio halos are also believed to be linked to shock waves from cluster mergers. There is a significant correlation between the presence of a radio halo in a cluster and a complex X-ray morphology or other merger indicators (Feretti & Giovannini 1996; Buote 2001; Schuecker et al. 2001). The different theoretical explanations for halos all seem to favor a developed state of the merger. Magnetic fields are expected to be stronger during the turbulent phase after a merger has proceeded past core passage (Dolag et al. 2002; Subramanian et al. 2005; Enßlin & Vogt 2005). This should lead to enhanced synchrotron emissivity in the post merger phase in nearly any radio halo model. In the *in situ acceleration model*, a certain level of turbulence is required to re-accelerate existing relativistic electron populations to higher energies (Giovannini et al. 1993; Brunetti et al. 2001, 2004; Gitti et al. 2002), also favoring a post-merger phase. In the case of the *hadronic secondary model* the radio emitting relativistic electrons are produced by inelastic collisions of relativistic protons with thermal protons (e.g. Dennison 1980; Vestrand 1982; Blasi & Colafrancesco 1999; Dolag & Enßlin 2000; Pfrommer & Enßlin 2004a). A merger shock wave which has already passed the cluster core is a prime candidate to have injected the necessary relativistic protons.

The low level of Faraday rotation measure dispersion ($RM_{\text{rms}} \approx 7 \text{ rad/m}^2$) of the relic can also be used to place constraints on the geometry of the merger. The expected rotation measure dispersion (see Eq. 40 of Enßlin & Vogt 2003) increases with the line of sight length L

$$\frac{d\langle RM^2 \rangle}{dL} = \frac{1}{2} a_0^2 n_e^2 \lambda_B \langle B^2 \rangle, \quad (1)$$

where, $a_0 = e^3/(2\pi m_e^2 c^4)$ is the usual Faraday rotation constant, n_e the electron density in the cluster core, λ_B the magnetic autocorrelation length, and B^2 the magnetic field strength. Inserting typical values for the A2256 cluster core electron density and radius from Mohr et al. (1999), $n_e = 3.5 \times 10^{-3} h_{70}^{1/2} \text{ cm}^{-3}$, $L = 350 h_{70}^{-1} \text{ kpc}$ (a core radius), with the size of the RM fluctuations equal to the synchrotron filament width visible in Figure 2) $\lambda_B = 30 h_{70}^{-1} \text{ kpc}$, and a very conservative field strength of $B_{\text{rms}} = 1 \mu\text{G}$ (as discussed in § 8) yields

$$RM_{\text{rms}} \approx 205 \frac{\text{rad}}{\text{m}^2} \left(\frac{n_e}{3.5 \times 10^{-3} \text{ cm}^{-3}} \right) \left(\frac{\lambda_B}{30 \text{ kpc}} \right)^{\frac{1}{2}} \times \left(\frac{L}{350 \text{ kpc}} \right)^{\frac{1}{2}} \left(\frac{B_{\text{rms}}}{1 \mu\text{G}} \right). \quad (2)$$

This estimate is much larger than what is observed, therefore the rotation measure dispersion favors a merger geometry in which the line of sight L through the high density ICM is significantly reduced. We note that the current data do not allow us to measure the RM fluctuation size on smaller scales due to the size of our beam. It seems unlikely, however that there are large RM fluctuations on very small scales as that would lead to depolarization within each beam due to the averaging of

different polarization angles across the beam. A comparison of the polarization fraction of the relics at 1703 MHz with that at 1369 MHz reveals a depolarization ratio ($DP = \%P_{1703}/\%P_{1369}$) of 1.08 across the relics which supports the argument against large RM variations on small scales. It therefore seems unlikely that we have significantly underestimated the RM_{rms} due to the limited resolution of our data. Using the best-fit model of Mohr et al. (1999) to determine the radial profile of the electron density, we find that even at the largest projected radial distance from the cluster core, the electron density is at most an order of magnitude lower than the central value, and thus the predicted RM_{rms} through the cluster would still be significantly larger than the observed value. The rotation measure dispersion, therefore, argues strongly in favor of the relic being located on the front side of the cluster.

The dynamical state of Abell 2256 is complex and is thought to consist of at least three merging systems based on optical velocity dispersions (Berrington et al. 2002; Miller et al. 2003) and shows evidence of three X-ray substructures (Sun et al. 2002). The main optical concentration appears roughly centered on the primary X-ray concentration, while the low velocity subcluster is thought to be associated with the cold X-ray concentration located along the southeast edge of the radio relic. The third (high velocity) optical system may represent a small group located to north of the cluster core and has not been detected in X-rays. The X-ray “shoulder” detected by Sun et al. to the east of the primary concentration is roughly centered on the halo and may represent an older merging component or internal structure in the central region of the primary cluster. The complex dynamical state of this system makes a unique determination of the merger history very difficult. We consider the small high velocity northern group to be unlikely to be related to the origin of the diffuse emission as halos and relics are nearly always associated with large mergers of systems with nearly equal mass ratios.

The X-ray emission associated with the subcluster shows a sharp edge toward the south which is consistent with a cold front (Sun et al. 2002). This suggests that at least some of the motion of this system is toward the south, although Sun et al. point out that the flat shape of the edge indicates that we are only seeing part of the edge due to projection effects. The merger geometry in Abell 2256 may be similar to Abell 754 rotated $\sim 180^\circ$ in the plane of the sky. In both Abell 2256 and Abell 754, the cold X-ray core of the merging component is bounded on one side by a steep surface brightness gradient. In Abell 754 the X-ray substructure does not appear to be associated with any large galaxy concentration. Markevitch et al. (2003) suggest that this cold core in A754 may have completely decoupled from its previous dark matter host and may be “sloshing” independently in the system. It is possible that a similar decoupling has occurred in Abell 2256 (M. Markevitch 2005, private communication) where the galaxy concentration thought to be associated with the merging subcluster is located to the north of the cold core. The morphology of the system suggests that the subcluster core may be traveling on a complex spiral trajectory about the primary cluster. Such a trajectory could result in the radio halo emission as well as relic location on the front-side of the clus-

ter with the shock propagation direction moving toward the northwest as suggested by the spectral index variation across the relic. The Z-shaped source may be an additional relic which has been revived by this merger. While the above merger scenario appears plausible to explain the observational parameters of A2256, we note that other scenarios could also be possible and detailed hydrodynamic simulations would be required to determine the validity of any merger scenario.

The two simplest merger scenarios for this system (shown in Figure 11) are: a) a current merger in a very early stage creating the radio relic with the radio halo being the remnant from an older merger event, or b) an advanced merger between the primary cluster and western subcluster where the merger shock has already passed the core of the primary to create both the diffuse halo and relic emission at the present location of the shock wave. We favor the scenario where the current major merger is responsible for both the diffuse halo and relic emission but we note that without detailed hydrodynamic simulations the current data do not allow us to exclude either model.

8. INTRACLUSTER MAGNETIC FIELD

The original goal of the polarimetry observations of Abell 2256 was to use the highly polarized radio relic as a screen against which to measure the intracluster magnetic field strength and scale. The observations revealed a small rotation measure of -44 rad m^{-2} which is consistent with the Galactic estimates. At the longitude of A2256 ($\ell = 110^\circ$) Faraday rotation measure maps show a large region of negative rotation measures running from latitudes of -40° up to at least $+10^\circ$ (Simard-Normandin et al. 1981; Johnston-Hollitt et al. 2004), thus it seems likely that the observed RM of A2256 at a latitude of $+32^\circ$ is related to this feature, and not the intracluster field. Further support for the Galactic origin of the observed RM comes from the very low RM dispersion across the relic (see § 7). Many more RM measurements in the region of Abell 2256 would be required to better constrain the Galactic RM contribution and determine the cluster contribution. We therefore do not attempt to measure an intracluster magnetic field strength using the Faraday rotation measure.

The magnetic field strength in clusters of galaxies can also be estimated through minimum energy arguments applied to the diffuse radio emission. We apply two different versions of such arguments. First, a conservative field estimate within the halo results from the *classical minimum energy condition*, which requires that the total energy in relativistic electrons and protons (assumed to be proportional to the electrons with a fixed ratio k_p) plus the magnetic energy has a minimum, with the constraint that the observed radio emission can be generated via the synchrotron process. This estimate can be applied in any scenario and can be regarded as a lower limit to the field strength (for conservative choices of k_p) unless one is willing to accept that there is much more energy in relativistic particles than in magnetic fields. Second, if radio halos are generated via the hadronic interactions of cosmic ray protons with the thermal gas, the proton-to-electron ratio k_p is not free any more, but

is fully determined by the physical processes such as the hadronic production, and the synchrotron and inverse Compton cooling of the produced electrons. This permits us to calculate a field estimate based on a *hadronic minimum energy condition*. The resulting field strength is only meaningful if the radio electrons are indeed of hadronic origin. The field estimate resulting from the hadronic condition will always be above that of the classical condition with a low adopted value for k_p .

We apply both the classical and the hadronic minimum energy criteria in the *nutshell* formulation of Pfrommer & Enßlin (2004b) to the radio halo of A2256. We adopt the following parameters: a conservative $k_p = 1$, a lower electron energy cut-off of $E_{e,\text{min}} = 0.1 \text{ GeV}$ (for the classical case), a cluster core radius of $350 h_{70}^{-1} \text{ kpc}$, a central electron density of $3.5 \times 10^{-3} h_{70}^{1/2} \text{ cm}^{-3}$ (Mohr et al. 1999), and a lower proton kinetic energy cutoff of 0.1 GeV (for the hadronic case). We note that the true spectrum of the halo is expected to display spectral curvature but this cannot be measured with current data, thus the results are given for three assumed spectral indices of the radio halo, namely $\alpha = -1.25$, $\alpha = -1.5$, and $\alpha = -1.7$. Confidence intervals are computed as described in Pfrommer & Enßlin (2004b) and mark the region within which the total energy of relativistic particles and fields stay within one e -folding from its minimum.

The classical minimum energy condition yields $B = 1.5_{-0.6}^{+0.9} \mu\text{G}$, $B = 2.4_{-0.8}^{+1.3} \mu\text{G}$, and $B = 3.2_{-1.1}^{+1.7} \mu\text{G}$ in the cases $\alpha = -1.25$, $\alpha = -1.5$, and $\alpha = -1.7$, respectively. The hadronic minimum energy condition yields $B = 3.3_{-1.2}^{+2.0} \mu\text{G}$, $B = 5.5_{-2.0}^{+3.1} \mu\text{G}$, and $B = 8.9_{-3.1}^{+4.8} \mu\text{G}$ in the cases $\alpha = -1.25$, $\alpha = -1.5$, and $\alpha = -1.7$, respectively. Due to the expected curvature of the halo spectrum, the lower magnetic field values are more likely representative for A2256. Both sets of results are in good agreement with Faraday rotation measurements of the magnetic field strength in galaxy clusters (Clarke et al. 2001; Carilli & Taylor 2002), and support our above scenario of a radio relic located in the cluster foreground on the basis of the weak Faraday dispersion for a μG level field.

The classical minimum energy fields we find are a bit higher than typical *equipartition* field values of $0.3 (1 + k_p)^{2/7} \mu\text{G}$ for radio halos given in the literature (e.g. Giovannini et al. 1993; Kim 1999; Thierbach et al. 2003). For A2256 Kim (1999) report $0.3 (1 + k_p)^{2/7} \mu\text{G}$, which is definitively lower than our estimate of at least $1 \mu\text{G}$. This difference is due to an important subtlety. In traditional equipartition calculations the lower cut-off of the electron spectrum is assumed to correspond to a frequency cutoff of 100 MHz , which corresponds for μG field strength to electron energies of 1 GeV , and to weaker field strength for even higher electron energies. However, there is no reason why the electron spectrum should cut off at such energies, or why it should know about our radio observational window (which closes shortly below 100 MHz). Therefore, we adopted an electron spectral cutoff at 0.1 GeV , which is motivated by the onset of effective Coulomb cooling below this energy as pointed out by Sarazin (1999). Having adopted a lower cutoff implies the presence of a larger non-thermal energy reservoir, which results in a

somewhat higher field strength.

9. SUMMARY AND DISCUSSION

We have presented new radio images of the diffuse synchrotron emission in A2256. In addition to the well-known radio relic region in this system, our new observations permit us to obtain the first detailed maps of the Mpc scale diffuse central halo emission.

Our polarization observations of this system show that the relic region has a high linear polarization fraction of up to 45% with an average polarization across the relic of 20%. The relic region contains extended polarization structures with nearly uniform field direction over more than half the length of the relic. We do not detect polarization associated with the radio halo or the steep spectrum Z-shaped source, and place upper limits on their polarization fraction of 16% and 2%, respectively. Our current data are limited to low resolution in order to be sensitive to the low surface brightness emission of the halo. If there are magnetic structures in the halo on scales smaller than our resolution (~ 50 kpc) the averaging of these structures in our beam could result in the low observed fractional polarization.

The Faraday rotation measure across the radio relic is remarkably uniform with a mean rotation measure of -44 rad m^{-2} which is consistent with our best available Galactic estimate from sources from the catalog of Simard-Normandin et al. (1981) within 15° of the cluster. The low mean RM and very low dispersion (7 rad m^{-2}) across the large region covered by the relic ($\sim 1125 \times 520$ kpc) both support a geometry with the relic located on the foreground side of the cluster with very little RM contribution from the intracluster medium. These data, as well as those of de Bruyn & Brentjens (2005)

on Perseus, represent the first opportunities to use radio polarimetry to determine the line-of-sight position of a merger shock wave in a galaxy cluster.

The radio relic region was found to have an average spectral index of $\alpha = -1.2$ between 1369 MHz and 1703 MHz with a radial steepening toward the cluster core. In the relic formation models, the diffuse emission is connected to shock waves generated by merger events. Given the large scale of the relic, it seems most likely that the emission is due to direct shock acceleration where the most recent acceleration (marking the the current shock location) is expected to be associated with the flattest spectrum emission. This suggests that (projected on the sky) the shock has moved from the southeast toward the northwest across the relic. It seems likely that the two diffuse non-thermal emission regions, the halo and the relic, are both related to the current violent hydrodynamical event. This would require the merger to be in an advanced stage where an associated merger shock has already progressed past core passage. We note, however, that detailed hydrodynamical simulations would be required to confirm this.

We thank the anonymous referee for helpful suggestions, Christoph Pfrommer for providing us with his minimum energy code, and Ming Sun for providing us with the *Chandra* image of Abell 2256. We thank Bruno Deiss, Uli Klein, Phil Kronberg, Maxim Markevitch, Neal Miller, Ming Sun, and Michael Thierbach for helpful discussions. TEC acknowledges support for this work from the National Aeronautics and Space Administration, primarily through *Chandra* awards GO4-5149x and GO4-5133x issued by the *Chandra* X-ray Observatory, which is operated by the Smithsonian Astrophysical Observatory for and on behalf of NASA under contract NAS8-39073. Basic research in radio astronomy at NRL is supported by the office of Naval Research.

REFERENCES

- Andernach, H., Han Tie, Sievers, A., Reuter, H.-P., Junkes, N., & Wielebinski, R. 1988, *A&AS*, 73, 265
- Bacchi, M., Feretti, L., Giovannini, G., & Govoni, F. 2003, *A&A*, 400, 465
- Bennett, C. L., et al. 2003, *ApJS*, 148, 1
- Berrington, R. C., Lugger, P. M., & Cohn, H. N. 2002, *AJ*, 123, 2261
- Blasi, P. & Colafrancesco, S. 1999, *Astroparticle Physics*, 12, 169
- Bridle, A.H., & Fomalont, E.B. 1976, *A&A*, 52, 107 (BF76)
- Bridle, A.H., Fomalont, E.B., Miley, G.K., & Valentijn, E.A. 1979, *A&A*, 80, 201
- Briel, U.G., & Henry, J.P. 1994, *Nature*, 372, 439
- Briel, U.G., Henry, J.P., Schwarz, R.A., Böhringer, H., Ebeling, H., Edge, A.C., Hartner, G.D., Schindler, S., Trümper, J., & Voges, W., 1991, *A&A*, 246, 10
- Brunetti, G., Blasi, P., Cassano, R., & Gabici, S. 2004, *MNRAS*, 350, 1174
- Brunetti, G., Setti, G., Feretti, L., & Giovannini, G. 2001, *MNRAS*, 320, 365
- Buote, D. A. 2001, *ApJ*, 553, L15
- Carilli, C. L., & Taylor, G. B. 2002, *ARA&A*, 40, 319
- Clarke, T. E., Kronberg, P. P., & Böhringer, H. 2001, *ApJ*, 547, L111
- Colafrancesco, S. 1999, in *Diffuse Thermal and Relativistic Plasma in Galaxy Clusters*, eds. H. Böhringer, L. Feretti, and P. Schuecker, MPR Report 271, 269
- Cordey, R. A. 1985, *MNRAS*, 215, 437
- Cornwell, T. J. & Perley, R. A. 1992, *A&A*, 261, 353
- de Bruyn, A. G. & Brentjens, M. A. 2005, *A&ASubmitted*, astro-ph/0507351
- Dennison, B. 1980, *ApJ*, 239, L93
- Dolag, K., Bartelmann, M., & Lesch, H. 1999, *A&A*, 348, 351
- Dolag, K., Bartelmann, M., & Lesch, H. 2002, *A&A*, 387, 383
- Dolag, K. & Enßlin, T. A. 2000, *A&A*, 362, 151
- Enßlin, T. A. 1999, in *Diffuse Thermal and Relativistic Plasma in Galaxy Clusters*, 275, arXiv:astro-ph/9906212
- Enßlin, T. A., Biermann, P. L., Klein, U., & Kohle, S. 1998, *A&A*, 332, 395
- Enßlin, T. A. & Brügggen, M. 2002, *MNRAS*, 331, 1011
- Enßlin, T. A. & Gopal-Krishna 2001, *A&A*, 366, 26
- Enßlin, T. A. & Vogt, C. 2003, *A&A*, 401, 835
- Enßlin, T. A. & Vogt, C. 2005, *A&ASubmitted*, astro-ph/0505517
- Feretti, L. 2002, *IAU Symposium*, 199, 133
- Feretti, L., Böhringer, H., Giovannini, G., & Neumann, D. 1997, *A&A*, 317, 432
- Feretti, L., Fusco-Femiano, R., Giovannini, G., & Govoni, F. 2001, *A&A*, 373, 106
- Feretti, L. & Giovannini, G. 1996, *IAU Symp. 175: Extragalactic Radio Sources*, 175, 333
- Feretti, L. & Giovannini, G. 1998, *Untangling Coma Bernices: A New Vision of an Old Cluster*, Proceedings of the meeting held in Marseilles (France), Eds. A. Mazure, F. Casoli, F. Durret, D. Gerbal, World Scientific Publishing Co. Pte. Ltd, P. 123
- Giovannini, G. & Feretti, L. 2000, *New Astronomy*, 5, 335
- Giovannini, G. & Feretti, L. 2002, *ASSL Vol. 272: Merging Processes in Galaxy Clusters*, 197

- Giovannini, G., Feretti, L., Venturi, T., Kim, K. T., & Kronberg, P. P. 1993, *ApJ*, 406, 399
- Giovannini, G., Tordi, M., & Feretti, L. 1999, *New Astronomy*, 4, 141
- Gitti, M., Brunetti, G., & Setti, G. 2002, *A&A*, 386, 456
- Govoni, F., Feretti, L., Giovannini, G., Böhringer, H., Reiprich, T. H., & Murgia, M. 2001, *A&A*, 376, 803
- Govoni, F., Murgia, M., Feretti, L., Giovannini, G., Dallacasa, D., & Taylor, G. B. 2005, *A&A*, 430, L5
- Hanisch, R. J., Strom, R. G., & Jaffe, W. J. 1985, *A&A*, 153, 9
- Harris, D. E., Stern, C. P., Willis, A. G., & Dewdney, P. E. 1993, *AJ*, 105, 769
- Hoefl, M., Brüggem, M., & Yepes, G. 2004, *MNRAS*, 347, 389
- Johnston-Hollitt, M., Hollitt, C. P., & Ekers, R. D. 2004, *The Magnetized Interstellar Medium*, 13
- Jones, C. & Forman, W. 1999, *ApJ*, 511, 65
- Kassim, N. E., Clarke, T. E., Enßlin, T. A., Cohen, A. S., & Neumann, D. M. 2001, *ApJ*, 559, 785
- Katz, N. & White, S. D. M. 1993, *ApJ*, 412, 455
- Kempner, J. C., Blanton, E. L., Clarke, T. E., Enßlin, T. A., Johnston-Hollitt, M., & Rudnick, L. 2004, in "The Riddle of Cooling Flows in Galaxies and Clusters of Galaxies", astro-ph/0310263
- Kempner, J. C. & Sarazin, C. L. 2001, *ApJ*, 548, 639
- Kim, K.-T. 1999, *Journal of Korean Astronomical Society*, 32, 75
- Liang, H., Hunstead, R. W., Birkinshaw, M., & Andreani, P. 2000, *ApJ*, 544, 686
- Masson, C.R. & Mayer, C.J. 1978, *MNRAS*, 185, 607
- Markevitch, M., et al. 2000, *ApJ*, 541, 542
- Markevitch, M., et al. 2003, *ApJ*, 586, L19
- Mesa, D., Baccigalupi, C., De Zotti, G., Gregorini, L., Mack, K.-H., Vigotti, M., & Klein, U. 2002, *A&A*, 396, 463
- Miller, N. A., Owen, F. N., & Hill, J. M. 2003, *AJ*, 125, 2393
- Miniati, F., Jones, T. W., Kang, H., & Ryu, D. 2001, *ApJ*, 562, 233
- Miniati, F., Ryu, D., Kang, H., Jones, T. W., Cen, R., & Ostriker, J. P. 2000, *ApJ*, 542, 608
- Mohr, J. J., Mathiesen, B., & Evrard, A. E. 1999, *ApJ*, 517, 627
- Pfrommer, C. & Enßlin, T. A. 2004a, *A&A*, 413, 17
- Pfrommer, C. & Enßlin, T. A. 2004b, *MNRAS*, 352, 76
- Reid, A. D., Hunstead, R. W., Lemonon, L., & Pierre, M. M. 1999, *MNRAS*, 302, 571
- Roettiger, K., Burns, J. O., & Pinkney, J. 1995, *ApJ*, 453, 634
- Roettiger, K., Burns, J. O., & Stone, J. M. 1999a, *ApJ*, 518, 603
- Roettiger, K., Stone, J. M., & Burns, J. O. 1999b, *ApJ*, 518, 594
- Roettiger, K., Loken, C., & Burns, J.O. 1997, *ApJS*, 109, 307
- Röttgering, H., Snellen, I., Miley, G., de Jong, J.P., Hanisch, R.J., & Perley, R. 1994, *ApJ*, 436, 654 (R94)
- Sarazin, C. L. 1999, *ApJ*, 520, 529
- Schindler, S., & Müller, A. 1993, *A&A*, 272, 137
- Schuecker, P., Böhringer, H., Reiprich, T. H., & Feretti, L. 2001, *A&A*, 378, 408
- Simard-Normandin, M., Kronberg, P. P., & Button, S. 1981, *ApJS*, 45, 97
- Slee, O. B. & Roy, A. L. 1998, *MNRAS*, 297, L86
- Slee, O. B., Roy, A. L., & Savage, A. 1994, *Australian Journal of Physics*, 47, 145
- Subramanian, K., Shukurov, A., & Haugen, N. E. L. 2005, *ArXiv Astrophysics e-prints*
- Sun, M., Murray, S. S., Markevitch, M., & Vikhlinin, A. 2002, *ApJ*, 565, 867
- Thierbach, M., Klein, U., & Wielebinski, R. 2003, *A&A*, 397, 53
- Venturi, T., Bardelli, S., Dallacasa, D., Brunetti, G., Giacintucci, S., Hunstead, R. W., & Morganti, R. 2003, *A&A*, 402, 913
- Venturi, T., Bardelli, S., Morganti, R., & Hunstead, R. W. 2000, *MNRAS*, 314, 594
- Vestrand, W. T. 1982, *AJ*, 87, 1266
- Vikhlinin, A., Markevitch, M., & Murray, S. S. 2001, *ApJ*, 551, 160
- West, M. J., Villumsen, J. V., & Dekel, A. 1991, *ApJ*, 369, 287

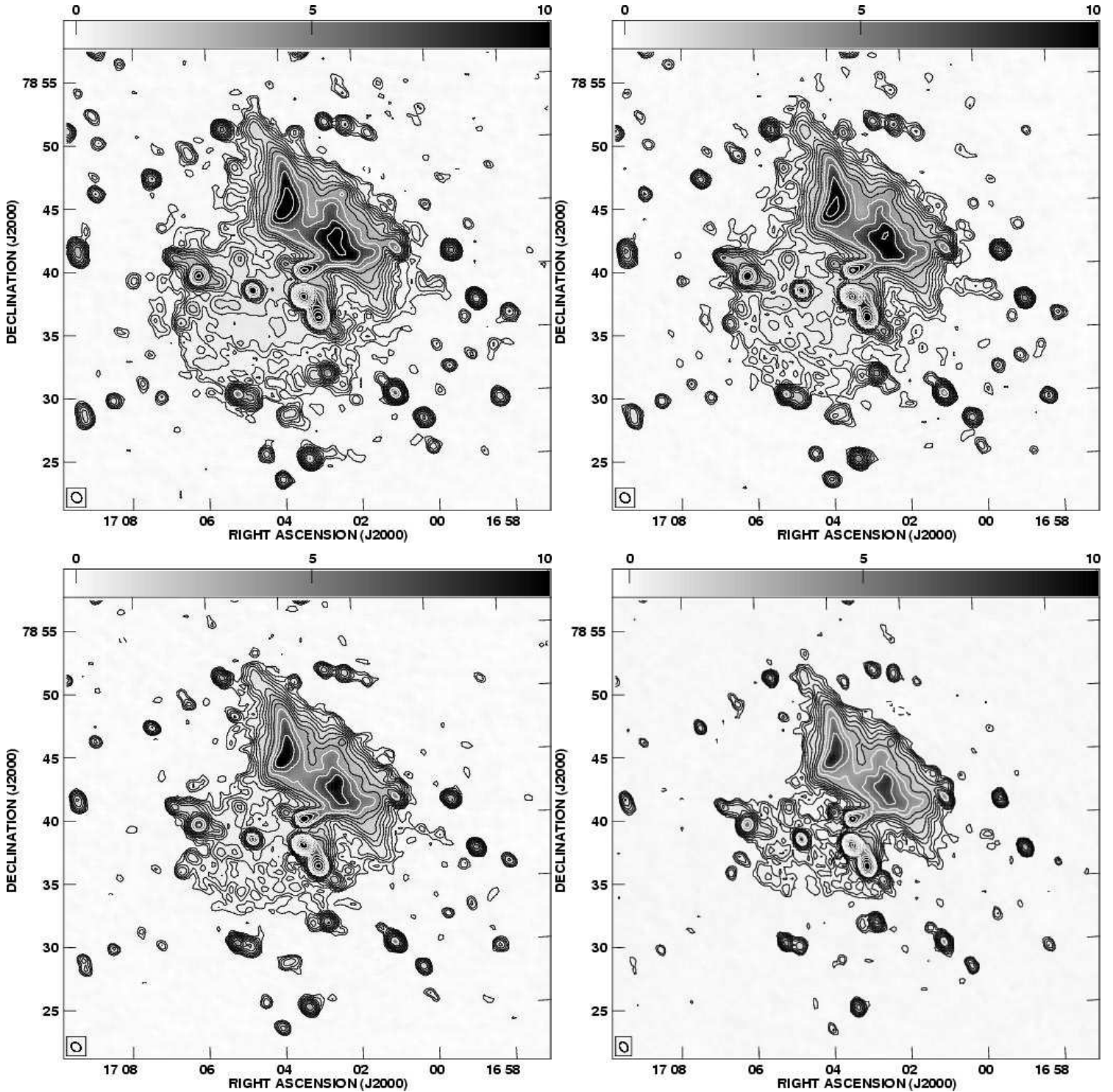


FIG. 1.— VLA D configuration total intensity greyscale and contours of Abell 2256. In addition to the compact sources, the diffuse emission associated with the peripheral relics and central radio halo is visible. All contours are plotted as $-3, 3, \dots$ times the rms level at $\sqrt{2}$ intervals. a) 1369 MHz contours. The rms level of $59 \mu\text{Jy beam}^{-1}$ and the restoring beam is $\sim 52'' \times 45''$. b) 1417 MHz contours with an rms level of $62 \mu\text{Jy beam}^{-1}$ where beam is $\sim 50'' \times 43''$. c) 1512.5 MHz contours with an rms level of $60 \mu\text{Jy beam}^{-1}$ and a beam of $\sim 49'' \times 39''$. d) 1703 MHz contours with an rms level of $68 \mu\text{Jy beam}^{-1}$ and a beam of $\sim 48'' \times 36''$.

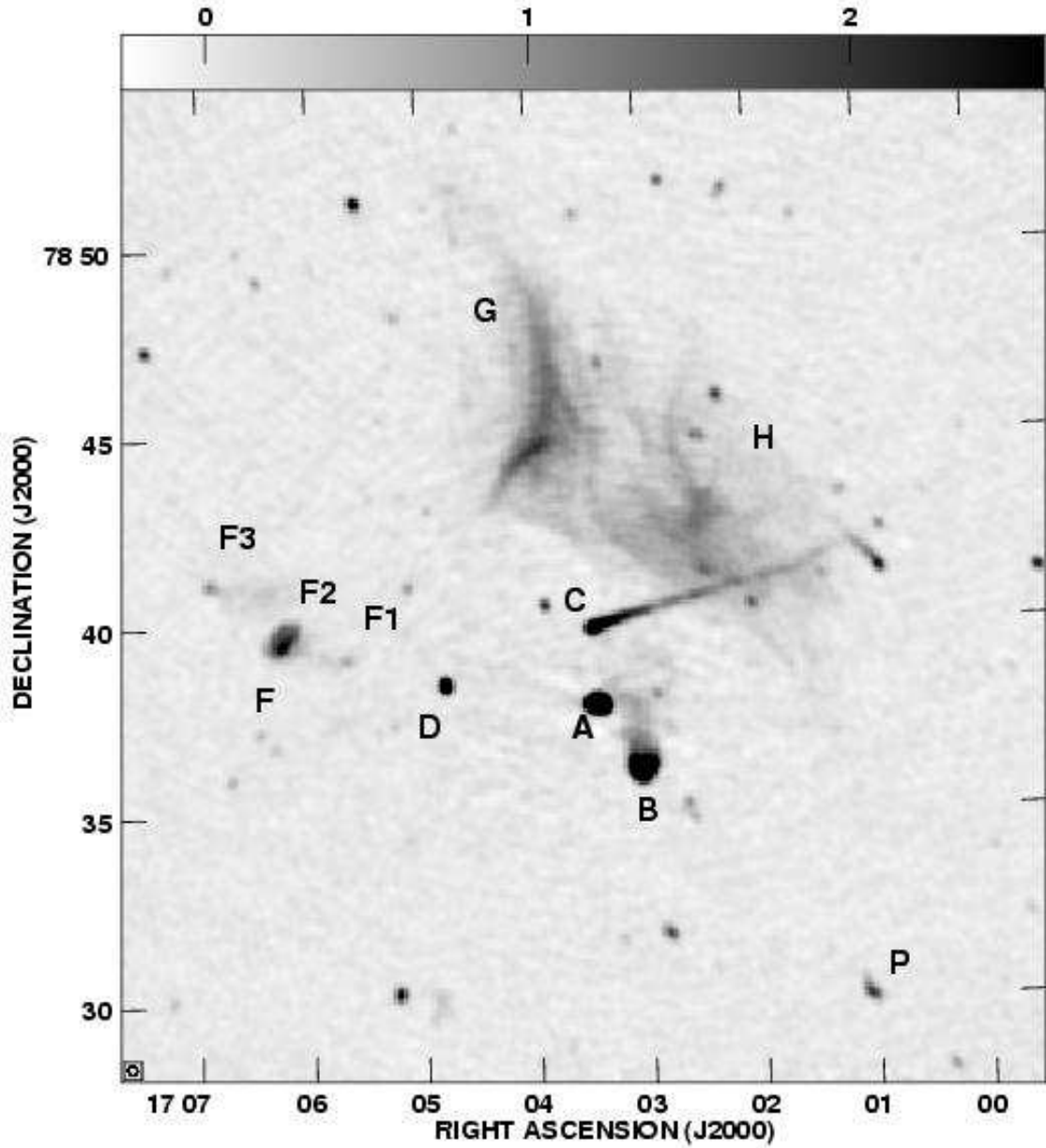


FIG. 2.— VLA C configuration 1369 MHz image of the central region of Abell 2256. Sources discussed in the text are labeled following the notation of BF76. The large scale diffuse halo and relic emission is resolved out due to a lack of short interferometer spacing in the C configuration data. In addition to the compact and extended sources, the relic region is seen to contain a number of synchrotron filaments. The rms level is $37 \mu\text{Jy beam}^{-1}$ and the beam is $\sim 15'' \times 14''$.

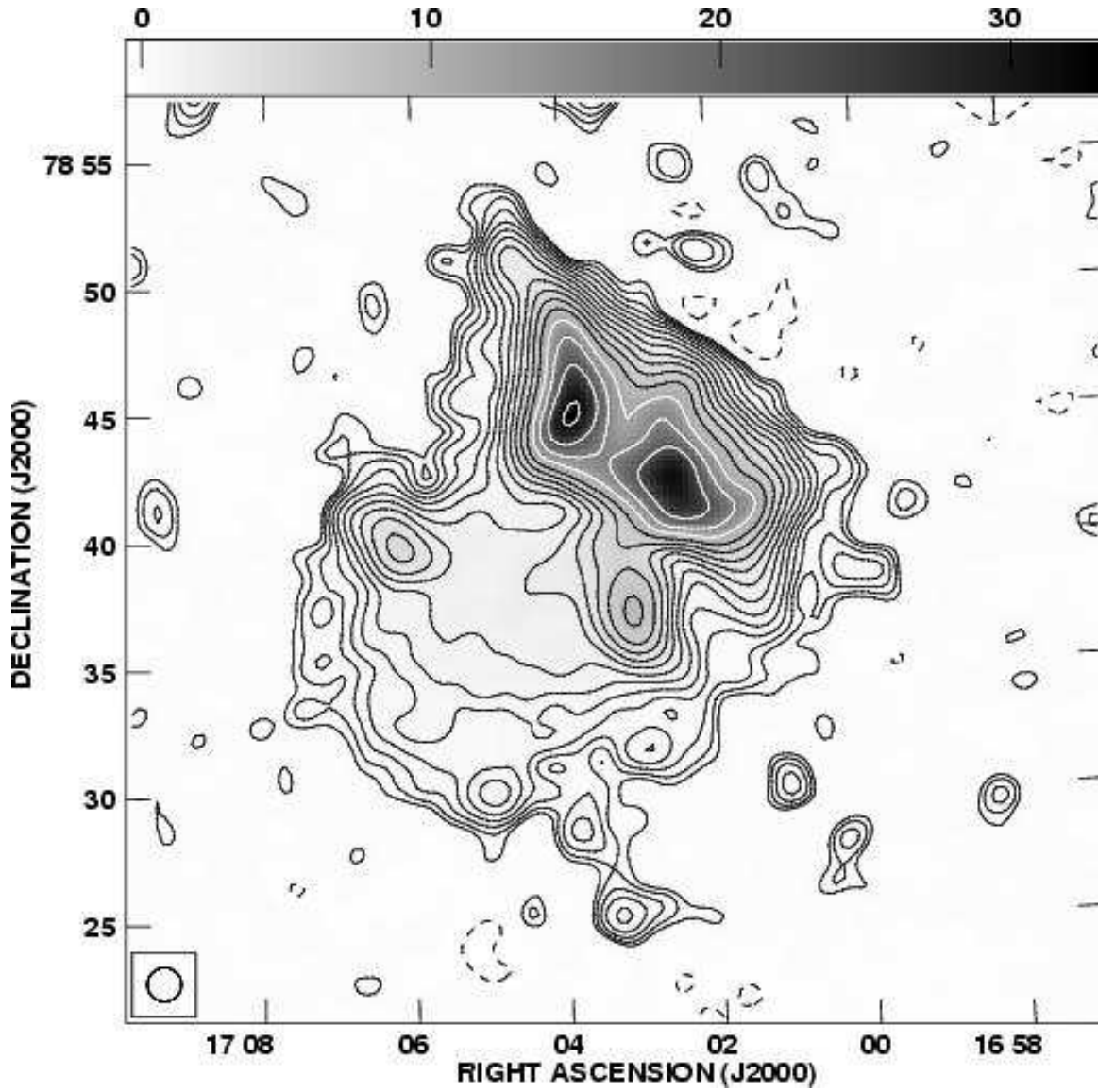


FIG. 3.— VLA 1369 MHz image of Abell 2256 after subtraction of discrete sources. The resolution is $80''$ and the noise level is $88 \mu\text{Jy}/\text{beam}$, with the contour spacing as in Figure 1. Several of the sources superimposed on the halo were extended over a large range of spatial scales and thus could not be completely removed from the image.

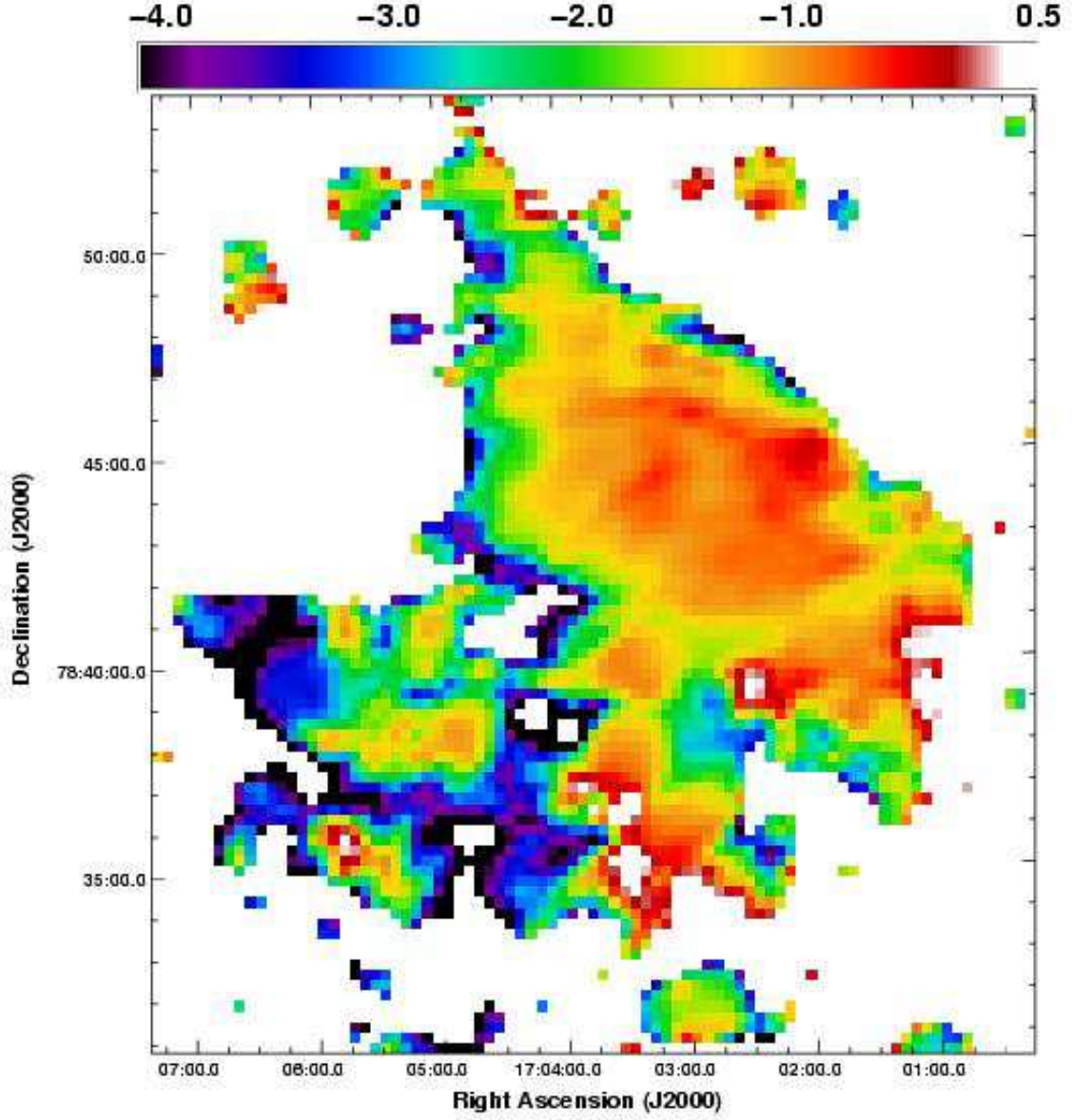


FIG. 4.— Spectral index map between 1369 MHz and 1703 MHz. The color bar at the top runs from spectral indices of -4.0 to +0.5 where $S_\nu \propto \nu^\alpha$. The spectral index of the relic region shows a steepening from the northwest to the southeast. Note that the spectral steepening across the tail of source C is also seen as a linear feature in the southwest portion of the map. We note that the spectral index over the diffuse halo is likely affected by the uv coverage issues discussed in § 5 and should not be estimated from this map.

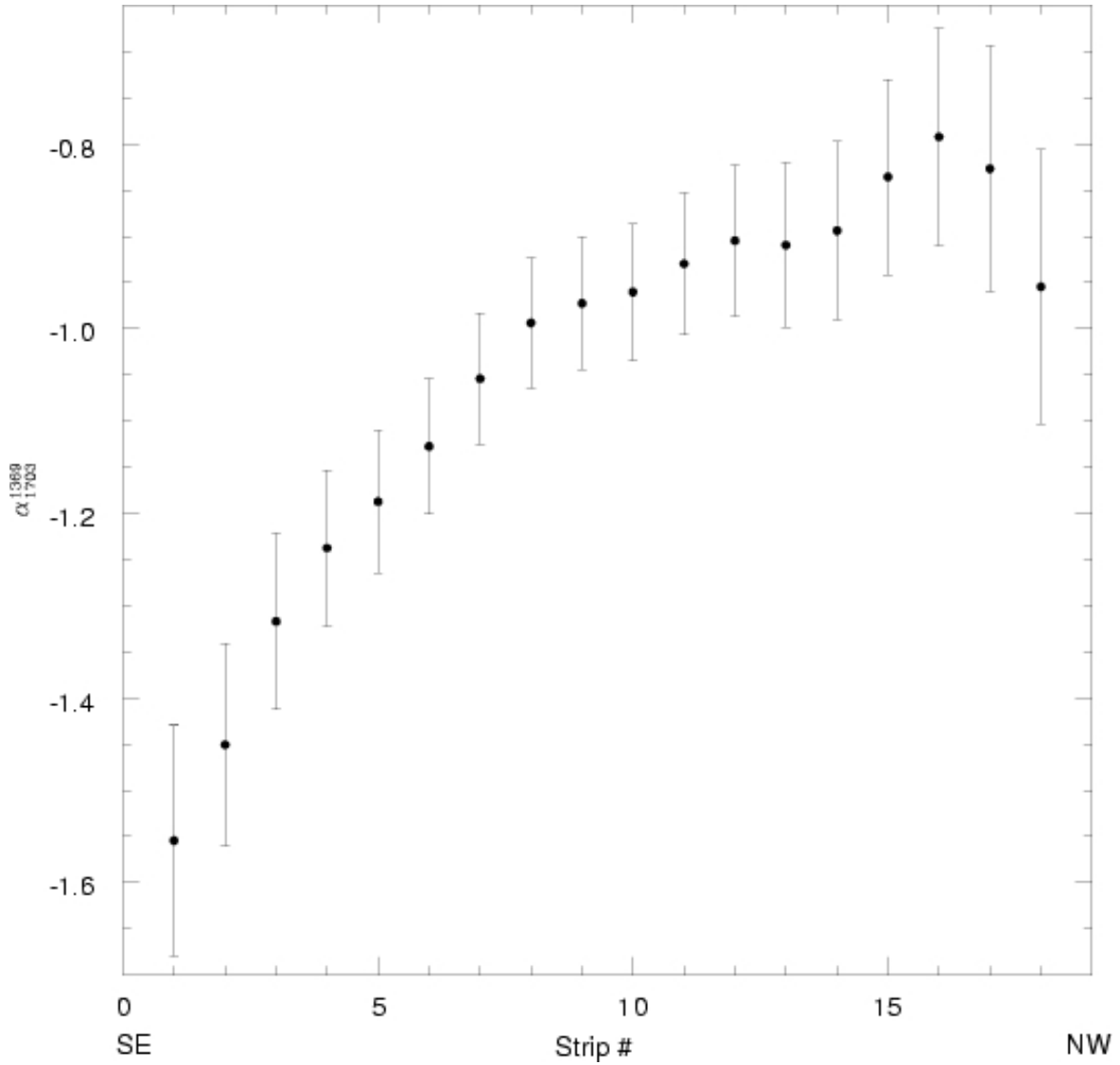


FIG. 5.— Average spectral index in 18 strips of width 6.5 parallel to the long edge of the relic. The average spectral index in each strip is plotted for strips 1 through 18 where strip 1 is near the SE relic edge, and strip 18 is near the NW relic edge. Note that while there are 18 strips plotted with the spectral index they are not all independent as there are 3 pixels per beam and thus roughly 6 independent resolution elements across the width of the region used to estimate the spectral index profile. The error bars show the 1σ errors on the spectral index.

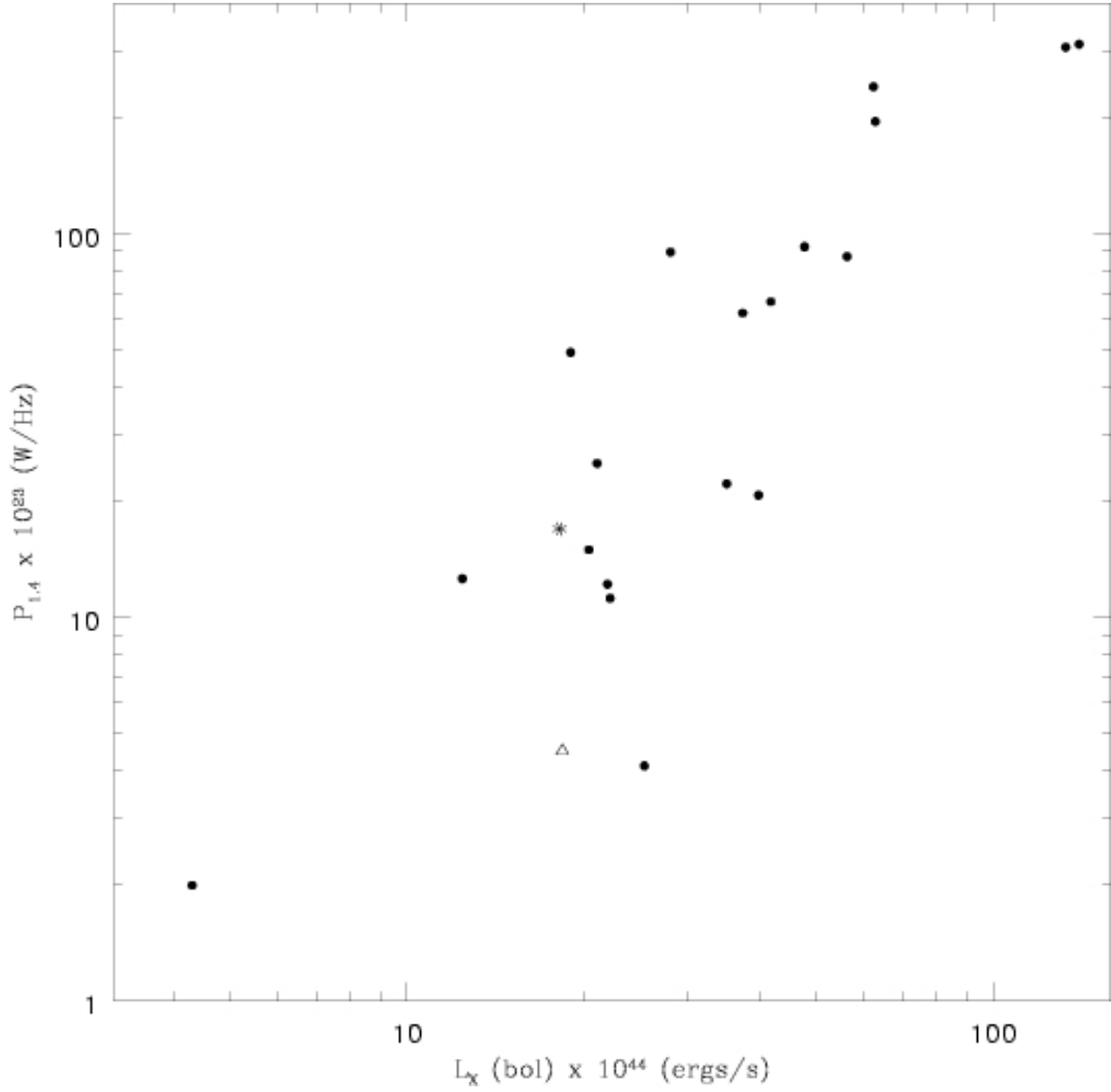


FIG. 6.— Plot of the $L_X - P_{1.4}$ relation for cluster radio halos. Filled black circles show halos from Govoni et al. (2001), Feretti (2002), Bacchi et al. (2003), and Venturi et al. (2003). The star shows the A2256 halo flux from this work and the open triangle is the A2256 halo flux reported in Feretti (2002). Note that we follow the convention in the literature for halo studies and adopt $H_0 = 50 \text{ km s}^{-1} \text{ Mpc}^{-1}$, $q_0 = 0.5$ in this plot.

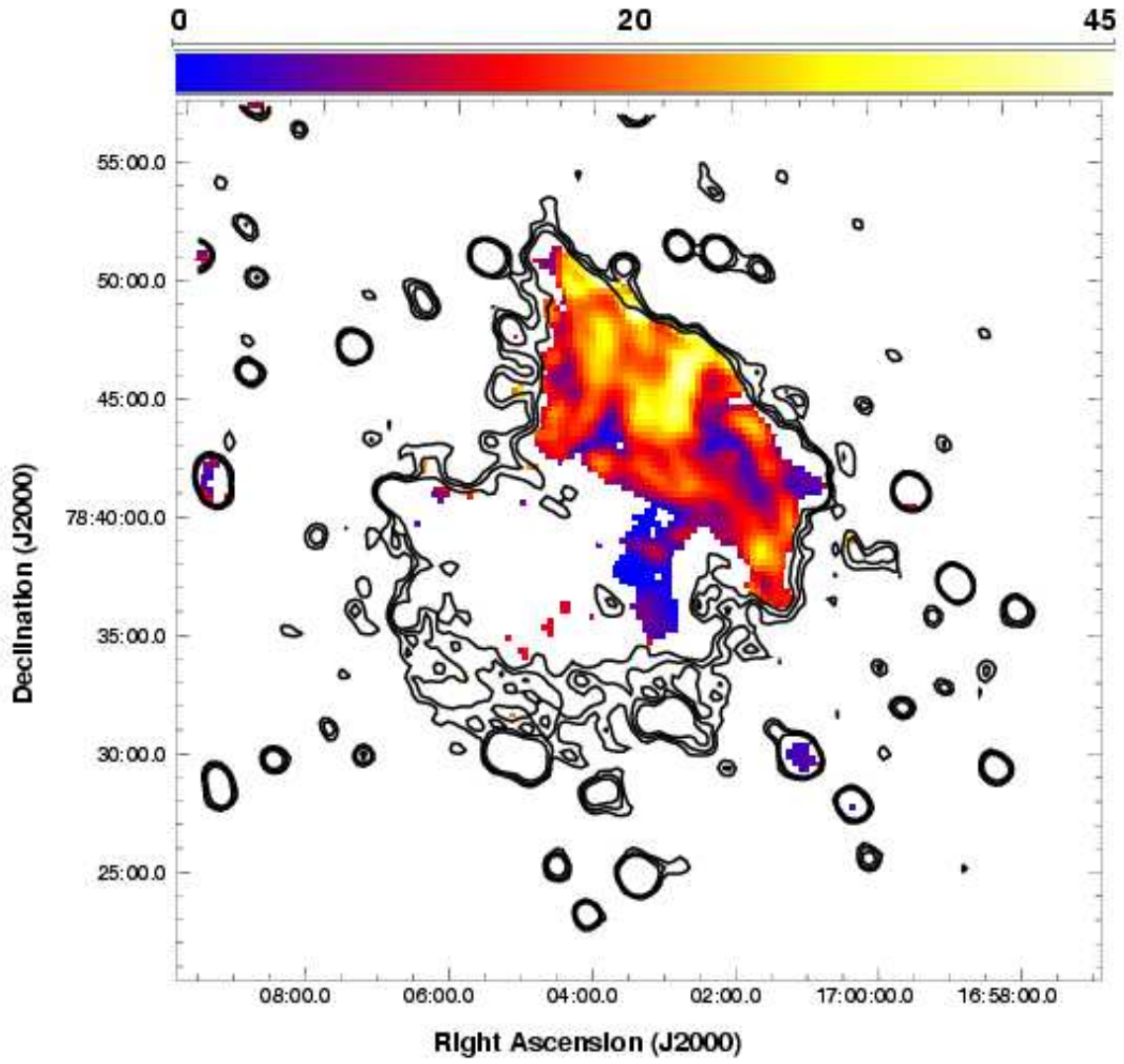


FIG. 7.— Fractional polarization is shown in color with the outer three contours from the VLA 1369 MHz D configuration data. The color bar at the top runs linearly from 0% to 45% polarization.

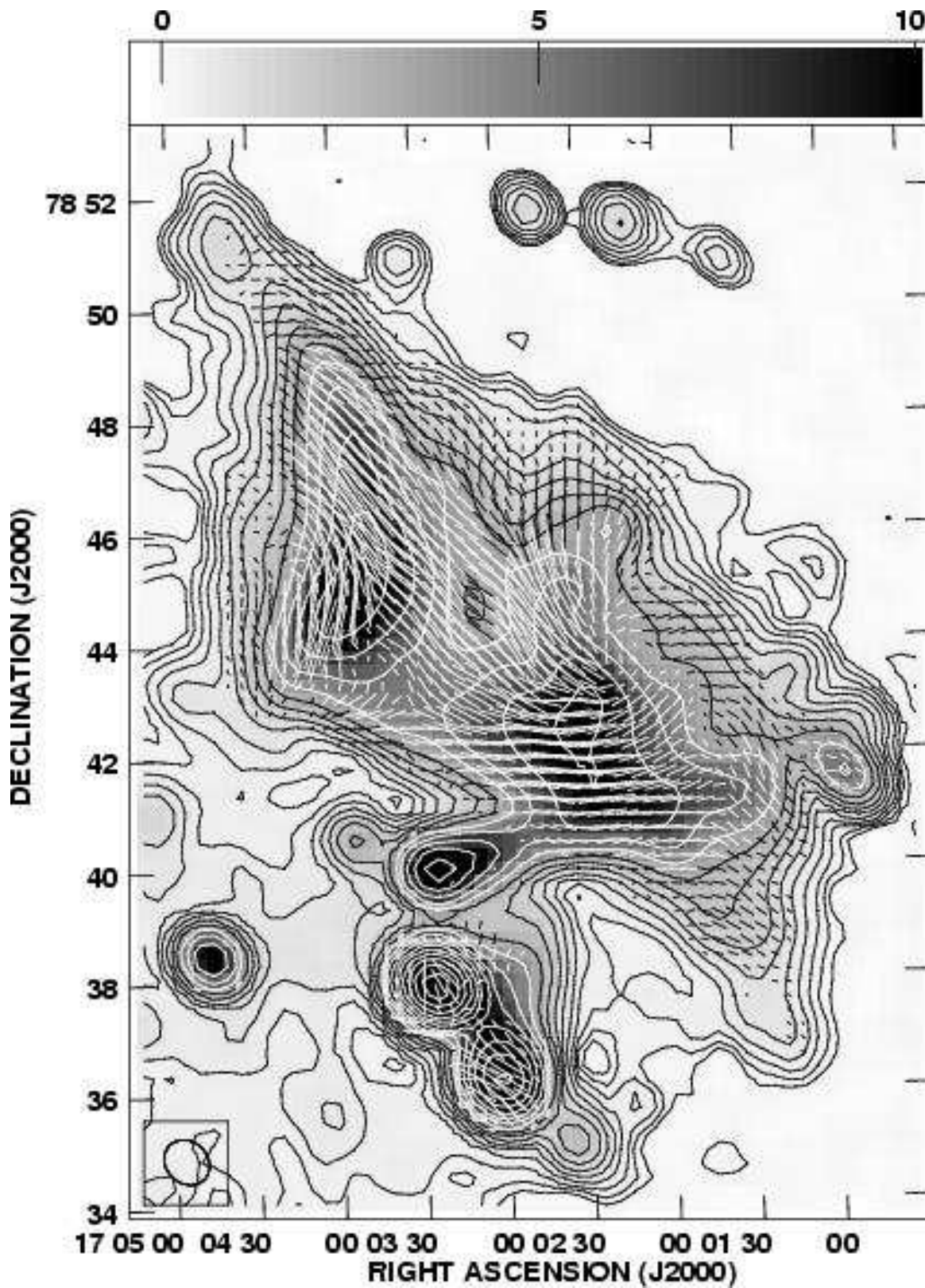


FIG. 8.— VLA 1369 MHz D configuration contours of the Abell 2256 relic region with the Faraday corrected magnetic field vectors overlaid. The polarization shows large regions of uniform direction over more than half of the length of the relic. Sources A and B (in the BF76 notation) are also polarized.

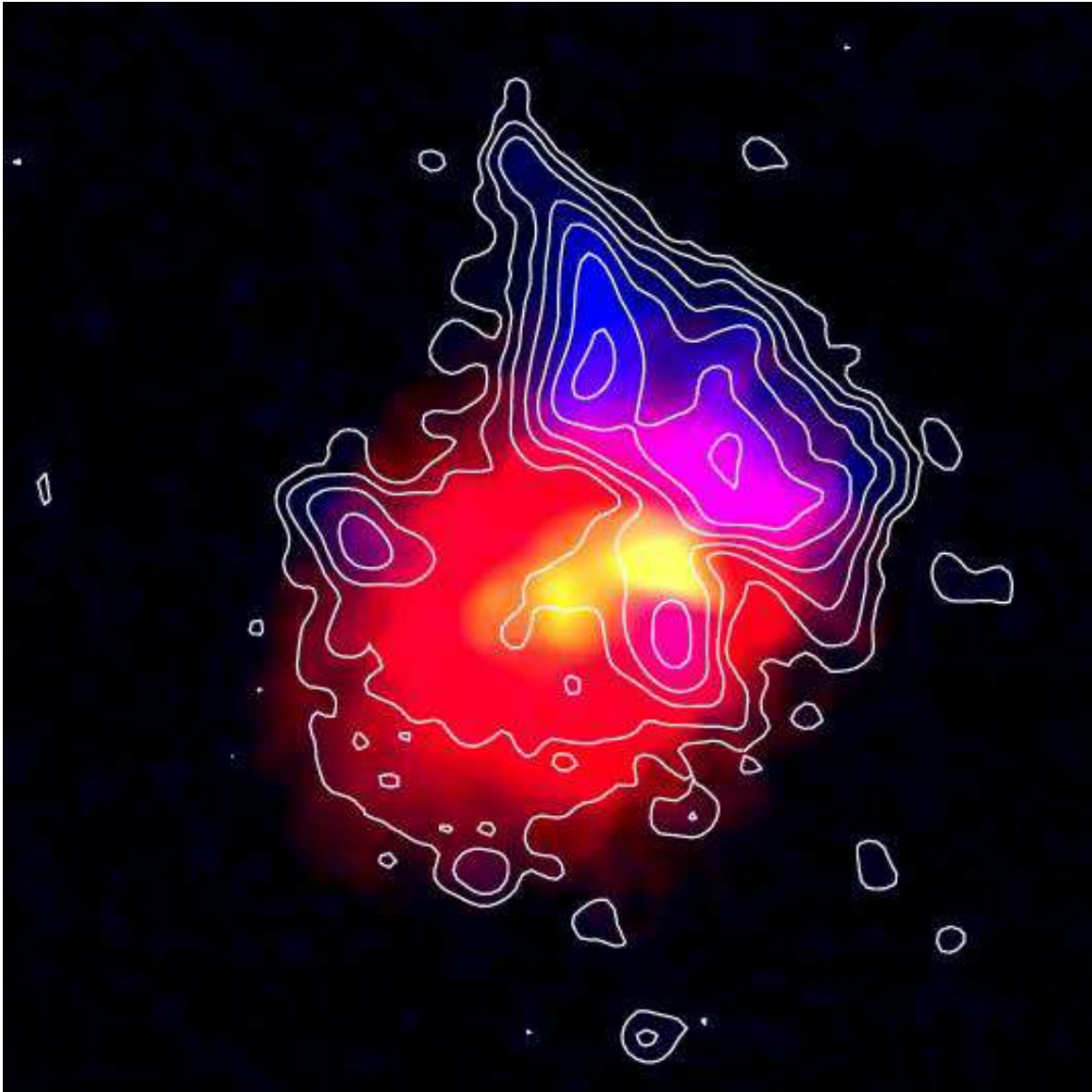


FIG. 9.— Three color image of the radio and X-ray emission in Abell 2256. Contours and blue emission show the 1369 MHz synchrotron emission from Figure 3, while the *Chandra* X-ray image is shown in red and green to reveal both the extended diffuse thermal emission as well as the three compact X-ray concentrations discussed in Sun et al. (2002). The large X-ray structure near the southeast edge of the relic is the cold core of the merging subcluster which is thought to be responsible for creating the diffuse radio emission.

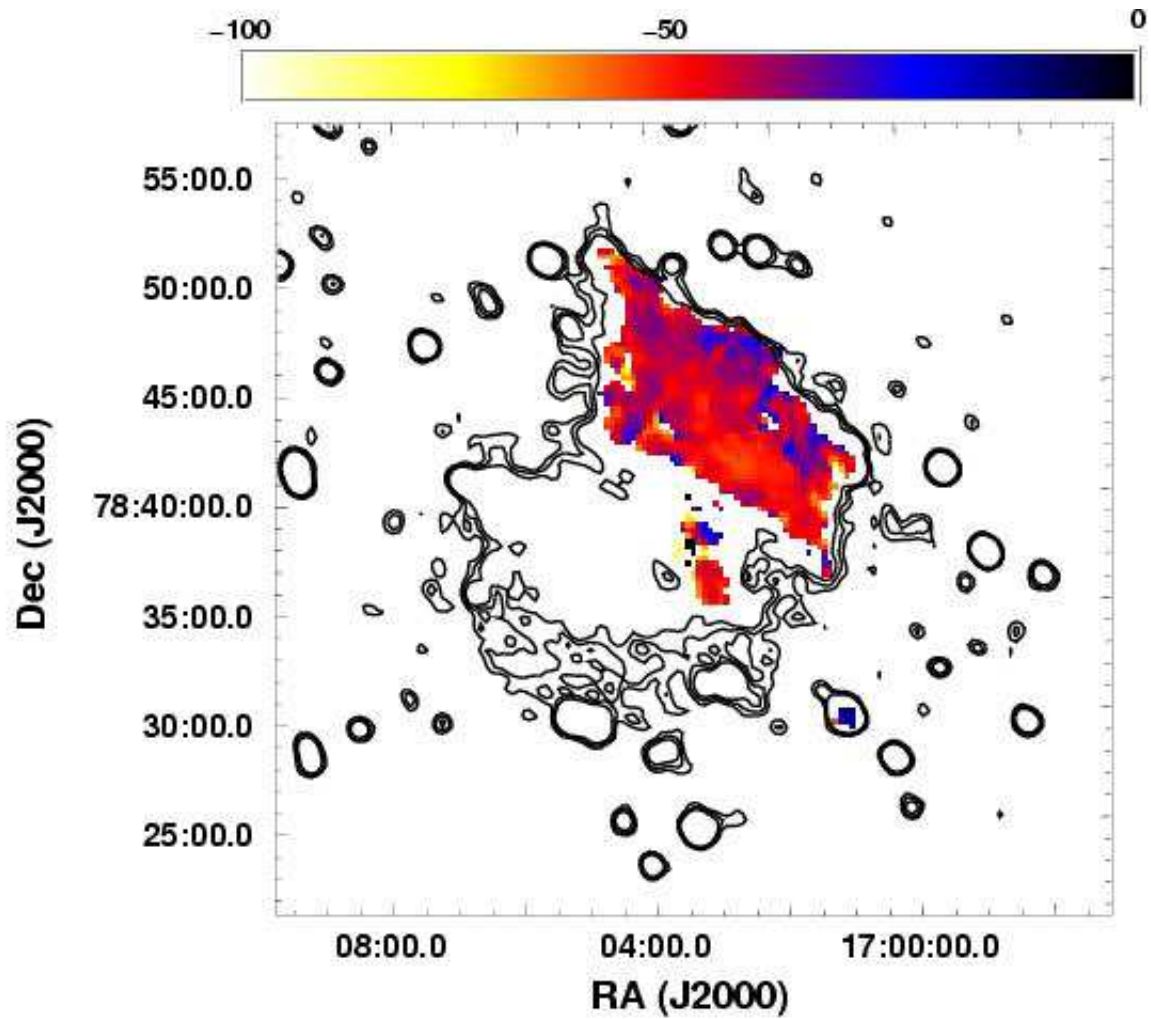


FIG. 10.— Faraday rotation measure map of the radio relics. Contours show the outer 3 contours from the VLA 1369 MHz D configuration image to provide a reference. The color scale shows the rotation measure running linearly from -100 rad/m^2 to 0 rad/m^2 . The rotation measure is relatively uniform over the majority of the relic with a mean rotation measure of -44 rad m^{-2} and a dispersion of 7 rad m^{-2} .

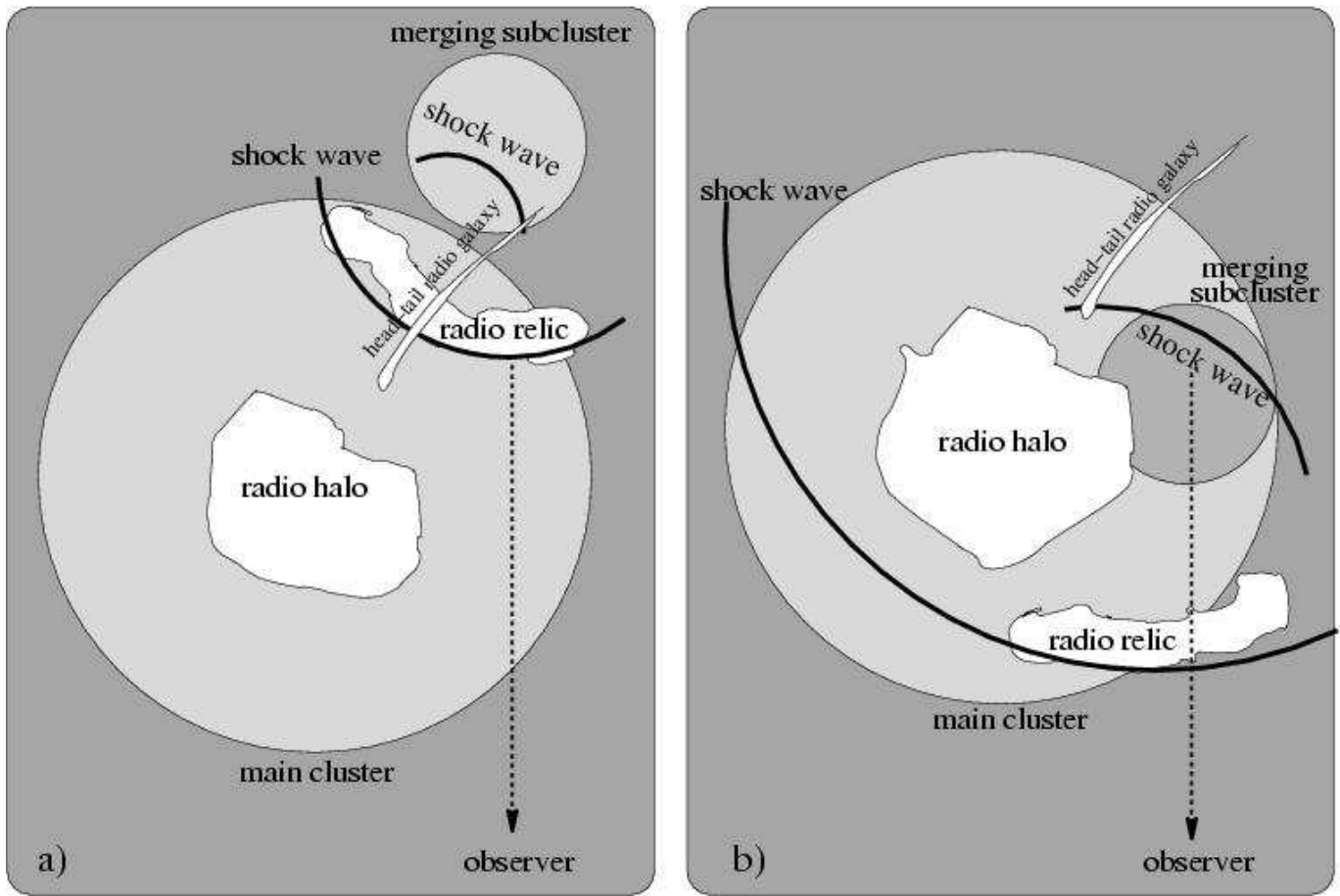


FIG. 11.— Possible geometries of the merger. Scenario a) is an early stage of the merger, where the shock waves have not had time to pass over the cluster cores, whereas scenario b) is in a more developed stage.

TABLE 1
VLA OBSERVATIONS.

Date	Array	Frequency MHz	Bandwidth MHz	Time h
1999 April 28	D	1369/1417	25/25	6, 6
1999 April 29	D	1512.5/1703	25/12.5	5, 3.5
2000 May 29	C	1369/1417	25/25	3, 3
2000 May 29	C	1512.5/1703	25/12.5	3.5, 3.5
2000 June 18	C	1369/1417	25/25	3, 3
2000 June 18	C	1512.5/1703	25/12.5	3.5, 3.5